

The treatment of Basic Oxygen Furnace (BOF) slag with concentrated solar energy

D. Fernández-González^{a,*}, J. Prazuch^b, I. Ruiz-Bustinza^c, C. González-Gasca^d, J. Piñuela-Noval^a, L.F. Verdeja^a

^a Department of Materials Science and Metallurgical Engineering, School of Mines, Energy and Materials, University of Oviedo, Oviedo, Asturias, Spain

^b Department of Physical Chemistry and Modelling, Faculty of Materials Science and Ceramics, AGH University of Science and Technology, Krakow, Poland

^c Universidad Politécnica de Madrid, Madrid, Spain

^d European University of Madrid-Laureate International Universities, Villaviciosa de Odón, Madrid, Spain



ARTICLE INFO

Keywords:

Concentrated solar energy
BOF slag
Steelmaking
Environment

ABSTRACT

Basic Oxygen Furnace (BOF) slag is one of the sub-products generated in the steelmaking process. This waste is characterized by its free lime and free magnesia contents that limit its application in construction. Moreover, the iron content in BOF slag of 14–30 wt% is a quantity which is problematic in the manufacture of cements. On the other hand, BOF slag is a source of available iron in the steelmaking industry. Concentrated solar energy offers a great potential in high temperature applications, so we used it to treat BOF slag. In this way, the slag was treated to stabilize it combining the free lime and free magnesia to give other phases (silicates, aluminates, and complex oxides), but also to transform iron into a magnetic phase that could be recovered through magnetic methods. The results demonstrate that the free lime and free magnesia reacted with silicates, aluminates, and ferrites to form stable phases which are not hydrated in the presence of water. Due to this, the treated BOF slag might find application in the construction industry. Furthermore, the iron was transformed into magnetite/maghemite, i.e. phases with magnetic properties.

1. Introduction

Basic oxygen furnace (BOF) slag is produced in the steelmaking process in quantities of 100–150 kg slag per ton of steel (Lan et al., 2017) during the oxygen converter process. This amount represents between 15% and 20% of the final volume of crude steel (Guo et al., 2018). 1691.2 Mt of crude steel were produced in 2017 according to the World Steel Association. This means that approximately 160–240 Mt of BOF slag are produced worldwide every year. For instance, 10 Mt of steel conversion slag were generated in 2010 in the European countries (Menad et al., 2014). These quantities pose a problem for the ironmaking and steelmaking industries, as BOF slags have a limited applicability. BOF slag comprises a mixture of different mineral phases, including calcium silicate, calcium ferrite and magnesia, iron oxide, free lime, and free magnesia (Gautier et al., 2013).

Blast furnace slag is used as a raw material in the cement industry, for instance, in the production of the hydraulic cement binder (Srinivasa Reddy et al., 2006). However, most of the BOF slag is still disposed in controlled landfills. For example, in Australia and New Zealand in the year 2000, 800,000 tons of BOF slag were produced

while 510,000 tons were used (64% utilization) in sealing aggregate, asphalt aggregate, base, subbase, construction fill, subsoil drains and grit blasting (Dippenaar, 2005). Some companies have tried to recover scrap iron present in BOF slag (Ferreira et al., 2002), being the final residue used in construction, e.g. in road pavements (Kambole et al., 2017). Others tried to enrich the slag with phosphorus to use it as a fertilizer in agriculture (Ferreira et al., 2002). Still others used BOF slag, due to its high Ca and Mg content, as a soil conditioner in agriculture (Annuziata Branca et al., 2014). Other applications include the utilization of BOF slag as a raw material in the production of glasses and glass-ceramics. In this way, Rabinovich (1982) produced a glass ceramic using BOF slag, and Ferreira et al. (2002) studied the production of glasses and glass-ceramics in terms of possible applications in floor and wall tile manufacturing.

The main disadvantage of BOF slag is its CaO content of 25–55 wt% (Shen and Forssberg, 2003), particularly the fraction of free lime and free magnesia as this problem causes swelling, excluding civil engineering applications (Gautier et al., 2013). The hydration and carbonation of free lime and free magnesia, occurring with aging, lead to swelling, which does not allow for using BOF slag in road construction

* Corresponding author.

E-mail address: fernandezdaniel@uniovi.es (D. Fernández-González).

(Gautier et al., 2013). On the contrary, the presence of CaO, MgO and MnO can be a positive factor in the steelmaking process, as they can replace part of limestone, dolomite and manganese ore and, consequently, reduce iron and steelmaking production costs. However, the presence of high quantities of P and S (Shen and Forssberg, 2003) is problematic in the iron and steelmaking process (Fernández-González et al., 2016; Fernández-González et al., 2017a, 2017b, 2017c, 2017d). Iron content may also be a problem in the production of clinker in the cement industry as standard clinker usually contains 2–3% Fe₂O₃, while BOF slags contain up to 20–30 wt% of iron (Gautier et al., 2013; Lan et al., 2017).

Iron is recovered from steel slags as their iron content can reach 14–30 wt% (Gautier et al., 2013; Lan et al., 2017). Typical methods include crushing, grinding, screening and magnetic separation. Lan et al. (2017) showed optimized recovery efficiencies of 93.20% magnetic iron in BOF slag. Guo et al. (2018) mixed BOF slag with an additive mixture containing kaolin and carbon powder. The objective of the treatment was to induce the reduction of ferric oxides. They obtained iron recovery efficiencies of more than 95%.

Solar energy, when adequately concentrated, offers a great potential in high temperature applications as well as in those involved in metallurgical processes (Fernández-González et al., 2018a, 2018b). This powerful energy source has been used in the recovery of valuable components from the steelmaking process. In this way, Ruiz-Bustinza et al. (2013) treated mill scale, which is produced in steelmaking in quantities of 5 kg of mill scale per ton of steel, in a fluidized bed solar furnace. The mill scale was pre-oxidized to hematite. After that, it was loaded into a fluidized bed solar furnace, where it was held for 4 h at 750 °C. In this way, they achieved the full conversion of the pre-oxidized hematite pellets into magnetite. The produced magnetite could be interesting as high-quality iron ore or for the aluminothermic welding of rails. Other researches discuss the reduction of hematite in the presence of graphite as a reducing agent. This was studied by Steinfeld and Fletcher (1991) and Steinfeld et al. (1993), who performed experiments to coproduce iron and synthesis gas by means of the Fe₃O₄ reduction with methane. Furthermore, Mochón et al. (2014), Fernández-González et al. (2018c, 2017e) and Fernández et al. (2015) also conducted experiments aimed at reducing hematite with carbon in a solar furnace. However, they observed that carbon was partially burnt under air atmosphere and it did not reduce the hematite. The main result of their experiments is that hematite can be thermally decomposed into magnetite at the temperatures involved in the process. Fernández-González et al. (2018c) observed a certain quantity of metallic iron in several experiments. Fernández-González et al. (2018c) also performed experiments in a solar furnace using iron ore sinter and coke. They observed the presence of metallic iron in all their experiments but in small quantities. Sibieude et al. (1982) evaluated the temperature and atmosphere in the decomposition of magnetite in a solar furnace. They observed that at 300 °C above the melting point of magnetite, 40% decomposition was achieved when the experiments were performed under air atmosphere, while full decomposition was reached when they used argon atmosphere.

As it was previously mentioned, BOF slags are characterized by a high iron content up to 14–30 wt% (Gautier et al., 2013; Lan et al., 2017), but also by the presence of free lime and free magnesia. Both these factors limit the usability of BOF slag in the cement manufacture and in construction. The main objective of this preliminary research was the use of concentrated solar energy to stabilize BOF slag. In other words, our aim was to eliminate both the free lime and the free magnesia through their transformation into silicates, aluminates and/or ferrites, due to which they would not be hydrated in the presence of water and swelling would be prevented. The second objective was the transformation of the iron oxides into magnetite/maghemitite, as these phases are magnetic. Apart from subjecting the slag to the solar beam, quartz sand was added with the purpose of changing the basicity of the slag (%(CaO + MgO)/%(SiO₂ + Al₂O₃)), which was supposed to

stabilize the slag.

2. Materials and methods

The experiments were performed in the 1.5 kW (maximum for 1000 W/m² DNI, Direct Normal Irradiance) vertical axis parabola medium size solar furnace located in Odeillo (France), which belongs to the PROMES-CNRS (Procédés Matériaux et Énergie Solaire – Centre National de la Recherche Scientifique). This solar furnace allows maximum concentrations of 15,000 times the incident radiation on a surface (focal point) of 15 mm in diameter, allowing maximum temperatures in excess of 3800 K. The regulation of the power applied in each experiment can be performed using a shutter. As we will see, similar values of power were used in all experiment by means of varying the shutter opening.

Two groups of experiments were performed with the BOF slag: the first group of three samples was treated as received (BOF 1, BOF 2 and BOF 3), while the second group of three samples with 6 wt% of quartz sand (BOF 4, BOF 5 and BOF 6). Treatments based on the addition of silica sand are usually aimed at changing the basicity of the slag. In this case, the added silica allowed us to reduce the basicity from around 4 in the original slag to a value below 3. Thus, the quantity of available silica to combine with the free lime and free magnesia was increased. Consequently, a displacement of the slag composition in the ternary phase systems FeO-CaO-SiO₂ and Fe₂O₃-CaO-SiO₂ is produced (see Fig. 1). The liquidus temperature of the slag, as indicated by Ballester et al. (2000), is between 1740 and 1779 °C, depending on the composition of the BOF slag. Performing the three experiments in each of the two groups was aimed at obtaining repeatability.

The BOF slag was analysed using X-ray fluorescence, the same as in the case of the quartz sand (Tables 1 and 2, respectively). We proceeded as follows to analyse the slag and ensure a representativeness of all the samples: (1) the sample was stirred to obtain a homogeneous sample; (2) the sample was disposed in a pile; (3) the pile was divided into four smaller piles; (4) the sample for the analyses was taken from one of the small piles. The same procedure was followed with all the analysed samples. The analyses were performed with a wavelength dispersive X-ray fluorescence spectrometer (Axios PANalytical) equipped with an Rh-anode x-ray tube with maximum power of 4 kW. All samples were measured in a vacuum with a 15–50 eV energy resolution. For a quantitative analysis of the spectra, the PANalytical standardless analysis package Omnia was used.

In our BOF slag, the iron content reaches 18%, which is in the range provided by Gautier et al. (2013) and Lan et al. (2017), i. e. 14–30 wt%. Both calcium oxide (II) and magnesium oxide (II) represent more than 50% of the slag. The presence of such quantities of calcium oxide (II) means important quantities of free lime (see Fig. 2). As it was mentioned above, the presence of free lime limits the utilization of BOF slag in construction because of the swelling processes occurring in the presence of water.

The chemical composition of quartz sand used as an additive is shown in Table 2. It mainly consists of silica with a certain quantity of alumina. The alumina content will not exceed 1% in the final product, although it contributes to reducing the basicity of the slag. The alumina will form aluminates with other phases at the involved temperatures.

The BOF slag was also analysed using the X-ray diffraction technique (Fig. 2). The X-ray diffraction measurements of powdered samples were conducted with an Empyrean PANalytical diffractometer using K α 1 and K α 2 radiation from a Cu anode. All measurements were performed with the Bragg-Brentano setup at room temperature with the 0.006° step size in the 5–90° 2 θ scanning range and the measurement time of 145 s for each step. The data analysis and peak profile fitting procedure were carried out using XPowder12 Ver. 01.02 (Database PDF2 (70 to 0.94)).

In the X-ray diffraction analysis of the BOF slag, we identified the following phases: portlandite ($\text{Ca}(\text{OH})_2$), hematite (Fe_2O_3), wustite

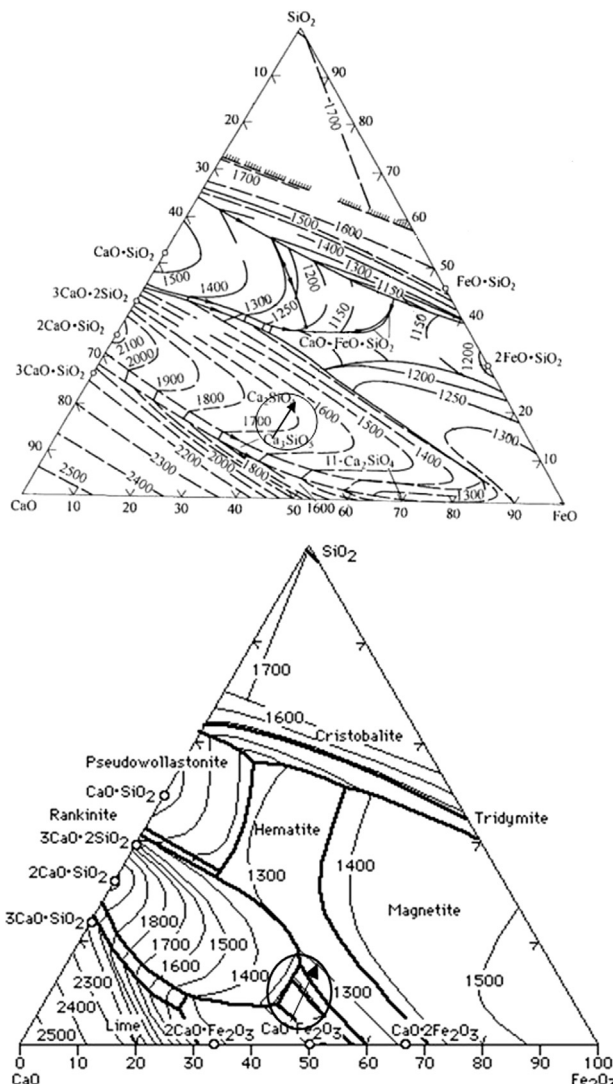


Fig. 1. The ternary phase systems FeO-CaO-SiO₂ (Zhu et al., 2013) and Fe₂O₃-CaO-SiO₂ (TAPP2.2; Levin et al., 1964).

Table 1
BOF slag chemical composition.

Element	Content (%)	Element	Phase	Content (%)
Ca	35.92	Na	Na ₂ O	0.272
O	33.15	Mg	MgO	1.565
Fe	18.01	Al	Al ₂ O ₃	2.745
Si	6.111	Si	SiO ₂	13.074
Mn	2.796	P	P ₂ O ₅	1.032
Al	1.453	S	SO ₃	0.605
Mg	0.9439	Cl	Cl	0.063
P	0.4506	K	K ₂ O	0.057
Ti	0.2683	Ca	CaO	50.259
S	0.2422	Ti	TiO ₂	0.448
Na	0.2018	V	V ₂ O ₅	0.191
Cr	0.1488	Cr	Cr ₂ O ₃	0.218
V	0.1069	Mn	MnO	3.610
Cl	0.06325	Fe	Fe ₂ O ₃	25.753
K	0.04719	Zn	ZnO	0.015
Sr	0.03023	Sr	SrO	0.036
Zr	0.02154	Zr	ZrO ₂	0.029
Nb	0.01983	Nb	Nb ₂ O ₃	0.028
Zn	0.01196			

Table 2
Quartz sand chemical composition.

Element	Content (%)	Element	Phase	Content (%)
O	49.46	Na	Na ₂ O	0.597
Si	34.49	Mg	MgO	0.473
Al	8.150	Al	Al ₂ O ₃	15.399
K	2.878	Si	SiO ₂	73.795
Fe	1.884	P	P ₂ O ₅	0.133
Ca	1.279	S	SO ₃	0.504
Na	0.4428	Cl	Cl	0.212
Mg	0.2850	K	K ₂ O	3.467
Mn	0.2318	Ca	CaO	1.789
Cl	0.2124	Ti	TiO ₂	0.339
Ti	0.2031	Cr	Cr ₂ O ₃	0.192
S	0.2017	Mn	MnO	0.299
Cr	0.1311	Fe	Fe ₂ O ₃	2.694
P	0.05796	Zn	ZnO	0.016
Rb	0.03623	Rb	Rb ₂ O	0.040
Zr	0.02657	Sr	SrO	0.013
Zn	0.01271	Y	Y ₂ O ₃	0.004
Sr	0.01108	Zr	ZrO ₂	0.036
Y	0.002853			

(FeO), kilchoanite ($\text{Ca}_9\text{Si}_6\text{O}_{21}\text{H}_2\text{O}$) and tremolite ($\text{Ca}_2\text{Mg}_5\text{Si}_8\text{O}_{22}(\text{OH})_2$). The free lime is represented by the portlandite (hydrated lime). Taking into account the above, the presence of hydrated phases could seem strange, but when this slag was removed during the converter, it was subsequently cooled in the presence of water.

The original slag was crushed and sieved into four granulometric fractions with different particle sizes corresponding to: > 4 mm, 2–4 mm, 1–2 mm and < 1 mm. The crucibles used in the experiments had the following dimensions: 55 mm in height, 30 mm in upper diameter, 25 mm in lower diameter and 3 mm in thickness of the walls, and they were manufactured in tabular alumina (Fig. 3). In this way, the free surface of the load was 24 mm in diameter while the solar beam was 15 mm in diameter. The fraction > 4 mm was rejected because part of the particles in this fraction had dimensions in the same order of magnitude as those of the solar beam, and this would limit the treated material. These three granulometric fractions were chosen to ensure a certain compactness with the purpose of minimizing the voids, and in this way reducing the projections of the material that could end outside the crucible, which was observed in the experiments performed by Mochón et al. (2014). If too fine-grained material is used, it could adhere to the glass hood used to protect the parabolic concentrator. Despite the granulometric fractions, projections/gas were observed in some experiments. This could be indicative of both the presence of volatile phases and the presence of particles of the smallest granulometric fraction. Consequently, three granulometric fractions (33%, 2–4 mm; 33% 1–2 mm; 33% < 1 mm) were mixed outside the crucible by stirring to ensure a homogeneous distribution of the particles and then charged into the crucible. The silica sand (1–2 mm) added to the second group of samples was also mixed with the three granulometric fractions of the slag by stirring to ensure a homogenous mixing and distribution of the particles, and then the mixture was charged into the crucible. The crucible was then put below the focal point and held for 15 min to similar values of power (see Table 3). The crucible was covered with a glass hood connected to a pump to avoid the projections of material (fine particles and volatile phases), which otherwise could settle in the parabolic concentrator (Fig. 3). However, gases released during the experiments were directly sent into the atmosphere without being collected. No gases were used in the experiments and the glass hood connected to the pump was provided in order to prevent potential damage or dirt concentration in the parabolic concentrator. Volatile phases were released during the experiments as gases were observed, and mass losses were measured in all experiments. Most of these mass losses and projections came from the slag and the silica, from the hydrated compounds and from some volatile compounds, such as sulphur

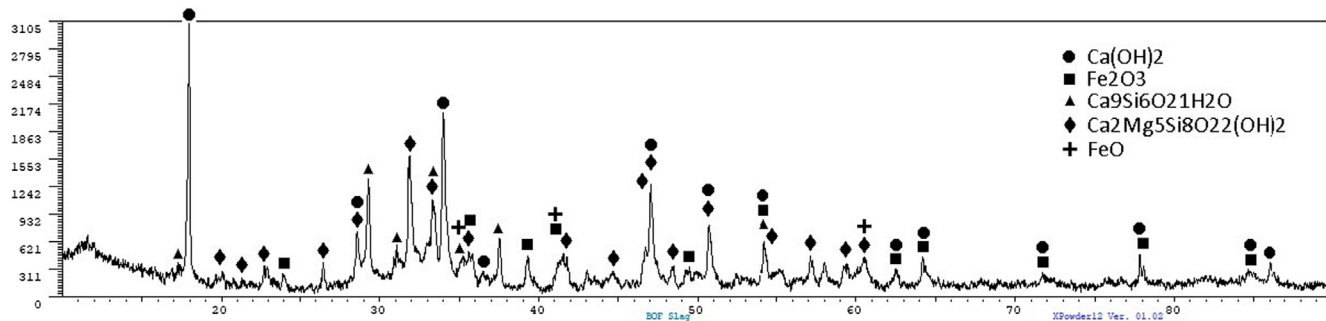


Fig. 2. The X-ray diffraction pattern of the BOF slag.

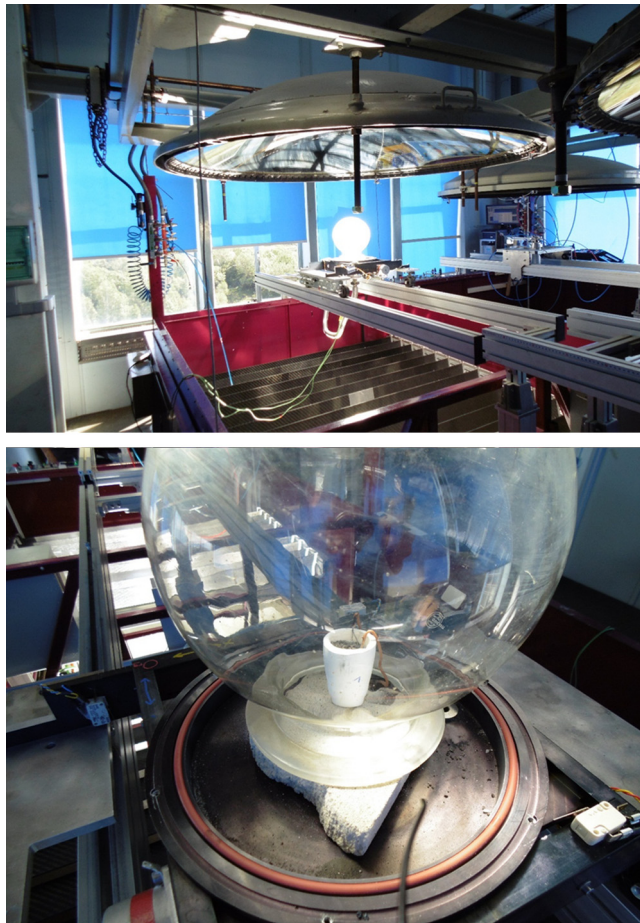


Fig. 3. The equipment used in the experiments.

Table 3
Experimental conditions.

Sample	Time (min)	Incident radiation (W/m ²)	Shutter opening	Power (W)
BOF 1	15	960	80	1152
BOF 2	15	949	90	1281.15
BOF 3	15	955	76	1088.7
BOF 4 (with silica sand)	15	974	80	1168.8
BOF 5 (with silica sand)	15	991	90	1337.85
BOF 6 (with silica sand)	17	989	76	1127.46

and part of the phosphorus. The sulphur was released during the experiments as it was not detected during the SEM-EDS analyses. In the case of the phosphorus, it was detected in some of the final products using SEM-EDS analyses. The removal of sulphur and phosphorus from the BOF slag would be beneficial for the ironmaking process. The treated product could be mixed with the sinter mixture without deteriorating its quality (Fernández-González et al., 2016; Fernández-González et al., 2017a, 2017b, 2017c, 2017d). Removing phosphorus and sulphur from the BOF slag was not the main objective of our experiments. However, as a result of these observations, the removal of phosphorus and sulphur should be further studied in future research. The aim of these investigations should be to study the elimination of sulphur and phosphorus from the slag, but sulphur and phosphorus must be captured before their release into the atmosphere.

Temperature was recorded using two type K thermocouples. One of the thermocouples, T1, was located outside the crucible at an average height of 27 mm, and the other, T2, inside the crucible at the bottom. The temperature measurements were used to control the progress of the process, i. e. to see when the process ended, and to determine if the temperatures were sufficiently high for the proposed process. It is obvious that to gain an exhaustive knowledge of the temperatures, we should have used other types of thermocouples (maybe type S or B thermocouples) and/or a solar blind pyrometer. However, the objective of our research was to demonstrate the feasibility of using concentrated solar energy to stabilize the BOF slag by eliminating the free lime. Future research in this line should be focused on studying the best conditions for the process: adjusted range of temperatures/power, exact additions of silica, best granulometric distribution, etc. The T2 thermocouple did not register the temperature of the entire process because it was melted during the process, but it provided information about the fast heating and indicated that the temperatures were higher than 1372 °C. The wires of the thermocouples were in contact with the inner wall of the crucible. The thermocouple was melted in the zone close to the free surface since when we removed the piece of the treated material which was 20–22 mm in depth and 24 mm in diameter, we found that the initial wires were broken in the layer of the unreacted material and re-welded in the zone of the treated material. In this way, the temperatures close to the crucible walls were higher than 1372 °C. Besides, as the solar beam, located exactly in the centre of the free surface, was 15 mm in diameter and heat distributes according to a Gaussian function, it can be concluded that the temperatures where the solar beam strikes the load were significantly higher than 1372 °C (hundreds of degrees higher than close to the crucible walls). The temperature reached at the point where the solar beam strikes the load is enough to melt the tabular alumina crucibles (the melting point of alumina is 2072 °C), as can be seen in Fig. 4. Thus, the temperatures are close to or higher than 2000 °C in the surface of the load and in the volume comprised within the load and a depth of 20–22 mm. According to Ballester et al. (2000) the liquidus temperature for BOF slags is close to 1750 °C, so we can confirm that the temperature was high enough to satisfy the objective of our research. The T1 thermocouple provided



Fig. 4. The crucible (tabular alumina), where the temperature was high enough to melt the walls.

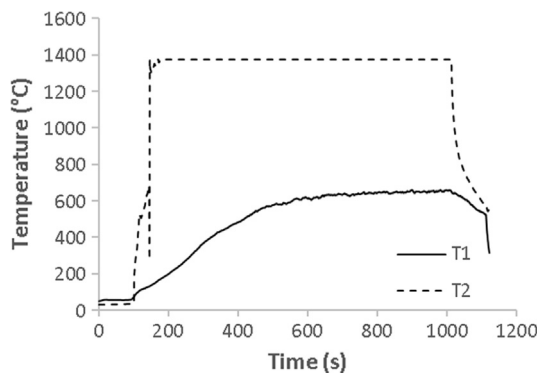


Fig. 5. The temperature registration of the T1 and T2 thermocouples (the BOF4 sample).

indirect measurement of the temperature. It was used to control the progress of the process, as when the temperature remains stable in the thermocouple T1, the process is supposed to be finished.

Fig. 5 shows the registration of the T1 and T2 thermocouples. T1 was used to control the process, while T2 provided information about the heating rate, and indicated that the temperatures were higher than 1372 °C. The sample was air-cooled down to room temperature. These heating and cooling rates allowed the presence of metastable phases, obtained at a high temperature, even at room temperature, but also restrained grain growth, which could be problematic in the case of iron phases (as the larger the size of the iron phase, the easier the way of collecting it). In the *Discussion* section we will explain the mechanisms involved in the process of treating BOF slag with concentrated solar energy.

3. Results

A total of 6 samples were obtained after the treatment with concentrated solar energy. Three experiments were performed in each group of samples to obtain repeatability: three using only BOF slag and the other three BOF slag + 6 wt% silica sand. The values of the experimental conditions are shown in Table 3. All the samples were subjected to similar values of power for 15 min. The value of incident radiation is provided by the measurement equipment and depends on the weather conditions (the values of incident radiation vary from one day to another and, apart from the presence of clouds, they depend on the moisture), but in our case, all experiments were performed under

similar conditions, as can be seen in Table 3. The shutter opening allowed us to control the power input by opening and closing it (0, the shutter closed; 100, the shutter fully open). The value of the applied power depends on: the shutter opening, the geometry of the parabolic concentrator and the incident radiation. As the geometry factor is a constant for all experiments, if the incident radiation changes, we can adjust the shutter to provide similar values of the power, as we see in Table 3 (the maximum power would be 1.5 kW under the best conditions, as we mentioned in the *Materials and Methods* section). The time chosen for the experiments was based on the measurement of the T1 thermocouple. It is assumed that the process is finished when the temperature in the T1 thermocouple remains stable (similar conditions were chosen in all experiments, and thus the duration of the treatment is the same).

The mass losses are related to the dehydration reactions as we identified portlandite ($\text{Ca}(\text{OH})_2$), kilchoanite ($\text{Ca}_9\text{Si}_6\text{O}_{21}\text{H}_2\text{O}$) and tremolite ($\text{Ca}_2\text{Mg}_5\text{Si}_8\text{O}_{22}(\text{OH})_2$) in the initial BOF slag. The mass losses are also related to the release of volatile phases (see the comments about the phosphorus and sulphur in the treatment of the BOF slag). The mass losses are listed in Table 4.

Good crystallization was observed in all the samples even with a naked eye (as shown in Fig. 6). The tetrahedral shape of the crystals is typical of magnetite crystals. The final product is magnetic. This factor together with the form of the crystals indicates that the iron was transformed into magnetite or another iron phase with magnetic properties (the initial BOF slag is not magnetic). The presence of magnetite (or any other magnetic iron phase, e. g. maghemite) indicates that, once milled, this magnetic iron phase could be collected through magnetic methods. We can also see the projections and the adherence to the crucible walls in Fig. 6.

The dimensions of the treated slag were recorded after the removal of the sample from the crucible. The volume of the treated material reached only 20–25 mm in depth. This could be a limiting factor for

Table 4
The mass changes in the samples treated with concentrated solar energy.

Sample	Initial mass (g)	Final mass (g)	Mass loss (%)
BOF 1	18.6	16.2	12.9
BOF 2	18.9	16.7	11.6
BOF 3	20.1	17.7	11.9
BOF 4 (with silica sand)	19.7	17.8	9.6
BOF 5 (with silica sand)	20.1	17.9	10.9
BOF 6 (with silica sand)	18.3	16.3	10.9



Fig. 6. A sample of BOF slag after the treatment with concentrated solar energy. Good crystallization can be observed.

scaling the process, although the employment of more powerful furnaces might solve the problem.

3.1. Results from the X-ray diffraction

The samples were analysed using the X-ray diffraction technique. The measurement conditions were the same as those previously mentioned.

3.1.1. BOF slag treatment without silica sand.

As it was mentioned above, three samples were obtained without adding silica sand. The experimental conditions are shown in Table 3. In this way, the sample was melted and then rapidly solidified with the presence of the stable phases (silicates of calcium and other phases containing iron). The presence of calcium silicates prevents swelling, which is associated with the volume change produced in the initial BOF slag when the free lime is hydrated. It would be crucial if the slag was to be used in construction (the slag is stabilized as free lime disappears). The conversion of the iron from the slag into a magnetic phase (maghemite/magnetite), which is easy to be retrieved from the slag, was the other objective proposed in this paper. Magnetite/maghemite are identified, and thus the final product, free of iron, would become a suitable candidate to be used in the production of cement (the magnetic phase could be used as an iron source in the production of steel, as it mainly contains magnetite/maghemite).

The existence of a liquid phase was observed even with a naked eye during the experiments. Liquid phase is available in the free surface of the load, since the temperature is higher in the area where the solar beam strikes the load and decreases as a Gaussian-shaped curve according to the diameter. The crucible was melted in some of the experiments (Fig. 4), and in others the sample was adhered to the crucible (Fig. 6). Consequently, the temperature was close to (or slightly higher than) 2000 °C. Considering the y-axis direction (if the origin is fixed in the surface of the load), the liquid phase reached 20–25 mm in depth. However, the material obtained after the treatment was not homogeneous; there was partial melting in the zones close to –25 mm, just as in the case of the sinter.

The X-ray diffraction patterns are shown in Figs. 7–9. For the X-ray diffraction analyses, the following procedure was used: (1) the treated sample was removed from the crucible; (2) it was cut into four pieces (two of them were used for the SEM-EDS analyses and the other two were used for the X-ray diffraction analyses); (3) two pieces were milled; (4) the powders were sent to the X-ray diffraction analyses. As a result, each X-ray diffraction is representative of each sample.

In this way, we see that complex silicates of calcium, aluminium, and magnesium (melilite, $\text{Ca}_8\text{Al}_6\text{MgSi}_5\text{O}_{28}$; and gehlenite, $\text{Ca}_2\text{Al}_2\text{SiO}_7$) were obtained after the treatment of the BOF slag with concentrated solar energy. Lime (CaO) was not detected in the analyses. Therefore, it is possible to say that the slag was stabilized during the experiments. Moreover, iron was found in the analyses as maghemite, which is a spinel ferrite with a structure similar to that of magnetite (it is a type of magnetite with vacancies), characterized by having magnetic properties. Thus, part of the iron could be collected through magnetic methods (the rest is found in the treated slag as magnesium ferrite, MgFe_2O_4 , which is also magnetic). The quantities of the phases identified in the X-ray diffraction analyses are listed in Table 5. The quantitative analyses were performed using XPowder12 Ver 01.02. The differences in the diffraction patterns are associated with crystallographic aspects, and with the presence higher or lower quantities of the amorphous phase. The quantitative analysis demonstrates the repeatability in the results.

3.1.2. BOF slag treatment with silica sand.

The other group of three samples was prepared using 6% of silica sand. The aim of adding silica, apart from modifying the basicity of the slag, was to displace the composition of the BOF slag towards compositions where the occurrence of silicates would be more favourable (Fig. 1). The peaks of the phases analysed using the X-ray diffraction technique are shown in Figs. 10–12.

In this set of experiments, we see that adding silica sand leads to the formation of fayalite ($(\text{Fe}^{2+})_2\text{SiO}_4$). This means that part of the iron, which would otherwise be transformed into maghemite, was, in this case, partially transformed into a phase that could not be collected through magnetic methods, i. e. fayalite. One of the main disadvantages of fayalite, apart from not being magnetic, is that the reduction of fayalite is much more difficult than the reduction of iron oxides. In fact, the iron ore market is mainly focused on hematite (Fe_2O_3) and magnetite (Fe_3O_4) (Sancho et al., 2000). Table 6 collects the quantitative analysis results of the phases identified in the X-ray diffraction pattern. The differences in the X-ray diffraction patterns are associated with crystallographic aspects. The results presented in Table 6 demonstrate the repeatability in the experiments. The addition of silica sand contributes to the stabilization of the slag but deteriorates the recovery of iron. Both types of experiments (with and without silica) allowed the equilibrium conditions to be restated by simply applying heat treatment, but without adding silica it is possible to transform iron into magnetite/maghemite.

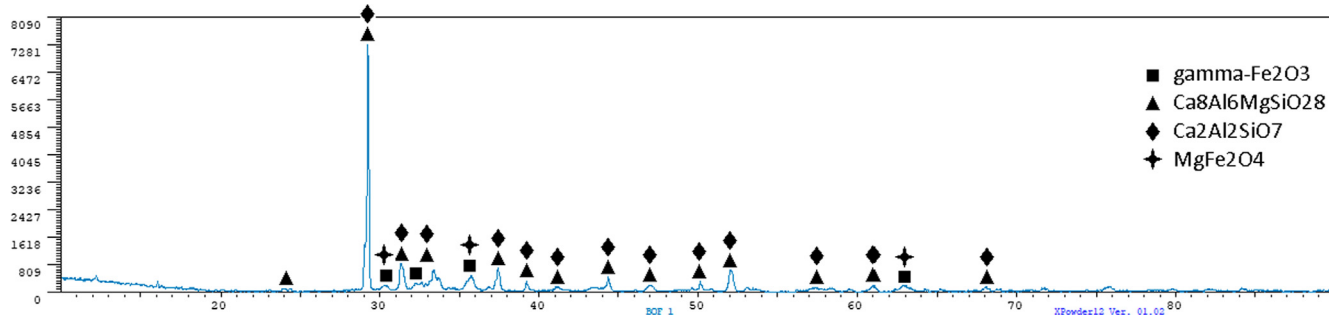


Fig. 7. The X-ray diffraction pattern for the BOF1 sample.

3.2. Results from the SEM-EDS method

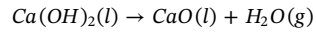
The samples were analysed using the SEM-EDS method. The carbon detected in the point analyses comes from adding this element to make the sample conductive for a scanning electron microscope. The samples analysed with the SEM-EDS method are representatives of the final products. It was observed that the free lime which was detected in the original sample later combined with silicon, aluminium, and iron to form silicates, silicoferrites and aluminates (Fig. 13, Table 7; Fig. 14, Table 8; and Fig. 15, Table 9). Thus, the lime was stabilized. The iron was detected as $\gamma\text{-Fe}_2\text{O}_3$ in the X-ray diffraction analyses. This phase is a spinel ferrite with the structure of magnetite, and usually occurs combined with magnetite. In fact, it is ferrimagnetic and resembles magnetite with vacancies. In Fig. 13, it is possible to see a zone of the BOF6 sample observed with the SEM where the magnetite, with the rhomboid shape, is in the middle of the image. It is possible to check by means of the point analysis (Table 7) that it is not pure magnetite. In fact, the presence of significant quantities of other elements indicates that substitutions were produced.

In the other samples or other zones of the samples, the structures are not as visible as in the case of Fig. 13. However, we can assume on the basis of the point analysis results that the magnetite and/or maghemite are iron-rich phases (see Point 3 in Table 7 and Fig. 13; and Point 1 in Table 8 and Fig. 14). The rest of the sample comprises silicates, aluminates, ferrites and complex silicoferrites of calcium and aluminium (see Point 1 and Point 3 in Table 9 and Fig. 15; and Point 2 and Point 3 in Table 8 and Fig. 14). These phases are typical of iron ore sinter (Fernández-González et al., 2017b, 2017c).

3.3. Discussion

The X-ray diffraction analysis of the initial slag indicates the presence of hydrated phases. The phases in the initial slag were hydrated because of the slag was removed from the converter and cooled with water. The presence of water in the initial samples explains the mass losses produced during the experiments, which were of approximately 10% (or slightly higher in some samples). If we use the HSC Chemistry 5.11, we can check that the decomposition of the portlandite ($\text{Ca}(\text{OH})_2$)

becomes favourable ($\Delta G^0 < 0$) at temperatures above 960 °C:



Dehydration reactions take place at the beginning of the process when the temperatures are lower. The sulphur and part of the phosphorus were released during the experiments because they were not detected in the final samples, i.e. sulphur was not detected in any of the samples, while phosphorus only in some of them (Point 2 and Point 3 in Table 7). This finding could be favourable for the reutilization of BOF slag in the sintering process. However, the development of a process based on solar energy only to eliminate sulphur and phosphorus from the slag does not seem reasonable. The costs involved in carrying BOF slag from a steelworks to a solar installation and back again to the sintering machine could be considerable, depending on both the location of the solar and steel plants. The solar treatment would be reasonable if the slag could be stabilized and the iron contained in it could be recovered separately, i.e. free of sulphur and phosphorus. Moreover, the quantity of BOF slag generated in the conversion process, amounting to 15% and 20% of the final volume of crude steel according to Guo et al. (2018), is relevant both to the design of solar equipment that could treat several hundreds of tons daily and to the transportation of the BOF slag to a solar installation. Nonetheless, the removal of sulphur and phosphorus should be further studied in order to eliminate them from the slag but also to avoid their release into the atmosphere. Thus, studying the removal of sulphur and phosphorus from BOF slags could attract researchers' interest if iron and slag could be simultaneously recovered and stabilized, respectively. Hence, low-sulphur and low-phosphorus high-quality iron ore and stabilized slag could be obtained at the end of the process from BOF slag. However, the released sulphur and phosphorus should be trapped with some chemicals.

We see that the iron content in the slag was close to 20 wt% (18 wt %, see Table 1). This iron content is low compared with the iron content of 60–65 wt% in the typical iron concentrates used in the ironmaking process (Fernández-González et al., 2017a), yet it is important as a material obtained (as by-product/waste) on the site in a manufacturing facility. The initial BOF slag contained iron mainly in the form of hematite (Fe_2O_3), according to Fig. 2 (but iron also appeared as wustite, FeO). Both iron oxides are not magnetic, and thus it is not possible to

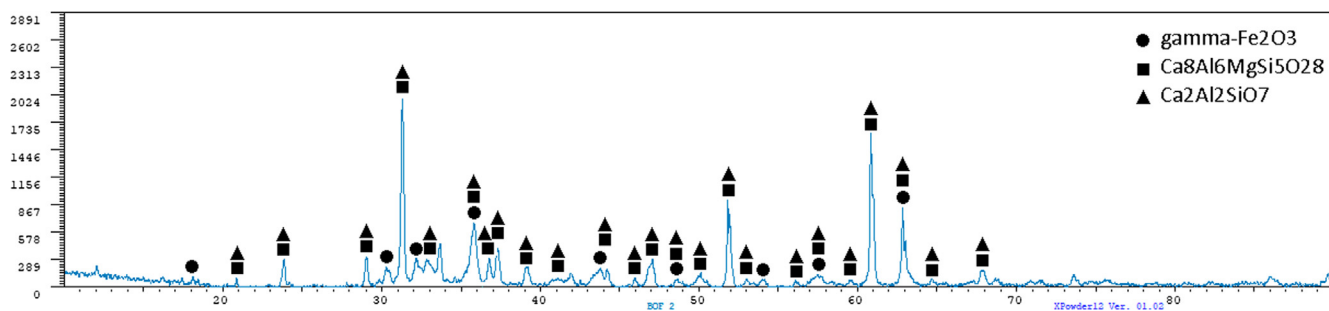


Fig. 8. The X-ray diffraction pattern for the BOF2 sample.

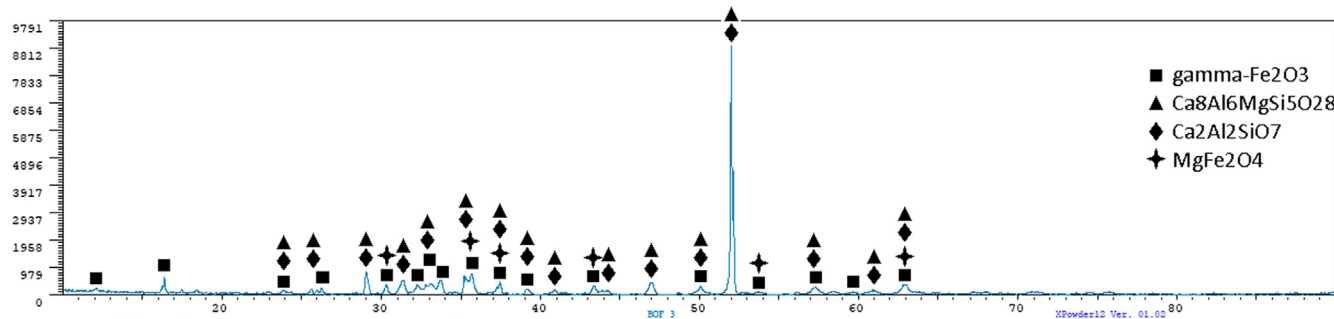


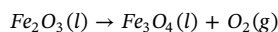
Fig. 9. The X-ray diffraction pattern for the BOF3 sample.

Table 5

The quantitative analysis of the x-ray diffraction samples (samples without silica sand).

	BOF1	BOF2	BOF3
γ-Fe ₂ O ₃ (maghemite)	17.40 ± 1.3	14.60 ± 4.8	14.0 ± 1.8
Ca ₈ Al ₆ MgSi ₅ O ₂₈ (melilite)	20.80 ± 1.2	20.30 ± 2.6	23.60 ± 1.1
Ca ₂ Al ₂ SiO ₇ (gehlenite)	19.70 ± 1.2	19.20 ± 2.6	22.30 ± 1.1
MgFe ₂ O ₄ (magnesioferrite)	19.20 ± 1.5		18.30 ± 1.9
Amorphous	22.90 ± 3.5	45.90 ± 4.6	21.90 ± 3.4

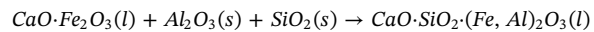
retrieve them using magnetic methods. This makes the recovery of iron from the initial slag difficult if the slag is not subjected to treatment (thermal or chemical, or combined). In the *Introduction* section, different treatments used to collect iron from BOF slag which have been proposed by several authors, apart from that proposed in this paper, were described. Ruiz-Bustinza et al. (2013), Mochón et al. (2014), Fernández et al. (2015) and Fernández-González et al. (2018c) observed that using concentrated solar energy, iron oxides can easily be transformed into magnetite/maghemite due to high temperatures. In this way, if iron phases are transformed into magnetite/maghemite, iron could be collected from slag by magnetic and gravimetric methods. Using the HSC Chemistry 5.11 we can check that the thermal decomposition (partial reduction) of hematite (Fe₂O₃) is thermodynamically favourable at temperatures above 1485 °C ($\Delta G^{\circ} < 0$), according to the reaction:



The presence of magnetite/maghemite is favourable due to the temperatures involved in the experiments with concentrated solar energy. This explains the magnetic behaviour of the samples. Thus, by milling and magnetic + gravimetric concentration, an iron-rich concentrate could be obtained and reintegrated in the sintering process. The iron-rich phase does not contain pure magnetite and maghemite as, in the point analyses, calcium and aluminium were detected, although only little amounts of phosphorus and no sulphur are detected. This iron-rich phase could be used as an iron concentrate for the sintering process. Apart from the iron concentrate, a product with low iron and

stabilized lime would be obtained. It could be used in construction (neither free lime nor free magnesia are found in this final by-product) or even in the production of cement. However, the use of this product in the manufacture of cement should be further studied to find out if it satisfies the requirements for its utilization as a raw material in this process. Moreover, the maximization of both the recovery of iron from slag should be also investigated.

The reactions involved in the process are solid-solid, solid-liquid, and liquid-liquid. The solid-solid reactions (between 750–780 °C and 1200 °C) would lead to the formation of the ferrites (more information on the reactions involved in the formation of ferrites can be found in Fernández-González et al. (2017b, 2017c)). At temperatures higher than 1200 °C the main reaction is solid-liquid Fernández-González et al. (2017b):



The product of the previous chemical reaction is known as SFCA (silicoferrite of calcium and aluminium) in the iron ore sintering process. A phase similar to the SFCA (closer to the calcium silicates) was identified in our experiments in Point 1 and Point 3 in Table 9 and Fig. 15; and Point 2 and Point 3 in Table 8 and Fig. 14. It is difficult to establish a specific composition for this phase because there is partial replacement of Ca²⁺ by Mg²⁺, Fe²⁺ by Mn²⁺, Fe³⁺ by Al³⁺ and Si³⁺, etc. (Fernández-González et al., 2017c).

The silica sand was added in an attempt to change the basicity of the slag by displacing the composition of the slag towards the formation of calcium silicates (see Fig. 1). However, fayalite appeared. This was detrimental for the recovery of iron from the slag because the iron was transformed into fayalite, but it is also a positive factor since the slag was stabilized.

One consideration that should be taken into account is based on the characteristics of the process. The kinetic constant for the chemical reaction k_q (Arrhenius type) is exponentially activated with the temperature, and thus processes that would take several hours in conventional furnaces can be performed in a solar furnace in several minutes. Moreover, another specific characteristic of the solar furnace, in particular of the heat transfer in this furnace, is that the heat is transferred in cents of seconds to a charge with a thermal diffusivity of $L^2 \cdot T^{-1}$.

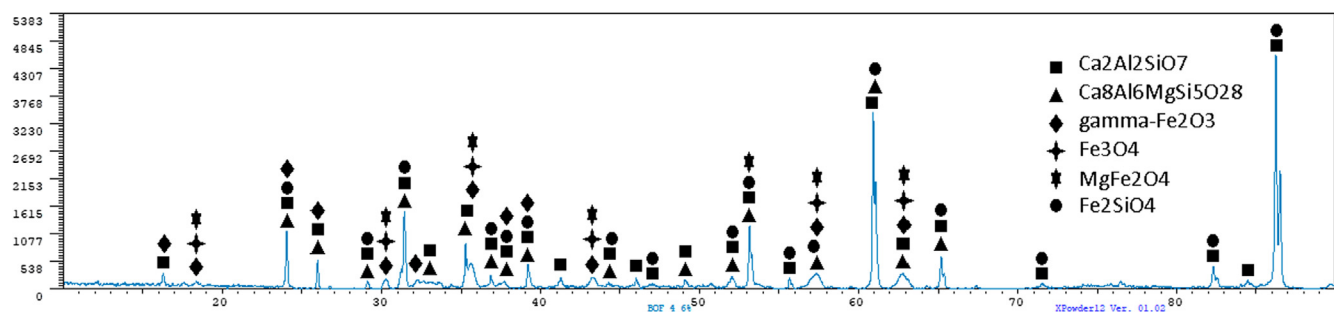


Fig. 10. The X-ray diffraction pattern for the BOF4 sample.

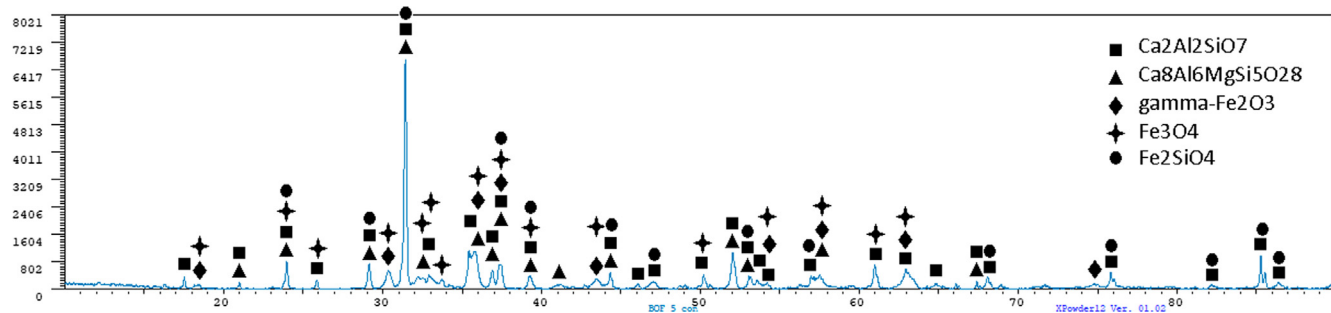


Fig. 11. The X-ray diffraction pattern for the BOF5 sample.

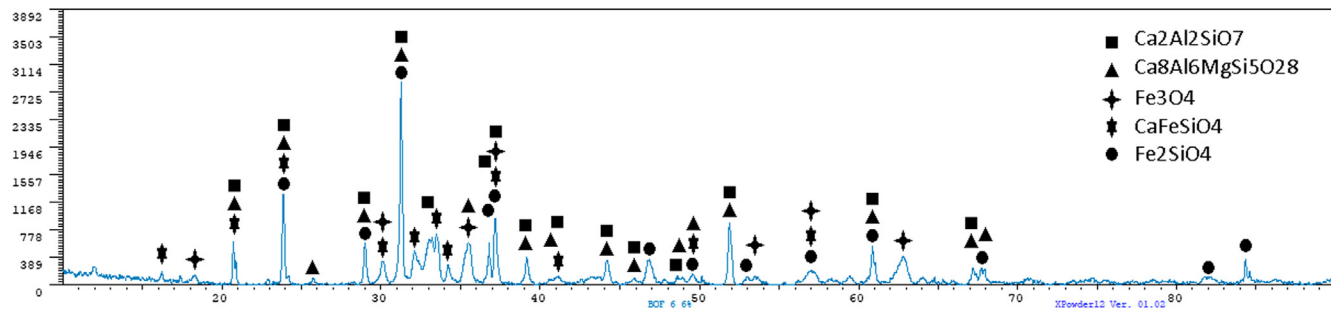


Fig. 12. The X-ray diffraction pattern for the BOF6 sample.

Table 6

The quantitative analysis of the x-ray diffraction samples (samples with 6 wt. % silica sand).

	BOF4	BOF5	BOF5
Fe ₃ O ₄ (magnetite)	9.30 ± 3.9	7.20 ± 4.9	7.70 ± 5.6
γ-Fe ₂ O ₃ (maghemite)	7.00 ± 3.9	5.40 ± 4.9	
Ca ₈ Al ₆ MgSi ₅ O ₂₈ (melilite)	8.30 ± 3.9	8.80 ± 4.5	18.20 ± 2.4
Ca ₂ Al ₂ SiO ₇ (gehlenite)	17.10 ± 1.7	23.10 ± 1.7	10.10 ± 4.8
MgFe ₂ O ₄ (magnesioferrite)	9.30 ± 3.9		
Fe ₂ SiO ₄ (fayalite)	17.70 ± 2.0	25.20 ± 1.8	13.90 ± 3.9
CaFeSiO ₄ (kirschsteinite)			6.40 ± 5.6
Amorphous	31.30 ± 4.0	30.30 ± 3.9	43.80 ± 4.5

Table 7

The results of the EDS analysis of the BOF6 sample from points shown in Fig. 13.

	Point 1 (wt. %)	Point 2 (wt. %)	Point 3 (wt. %)
C	2.02	2.46	1.88
O	28.43	29.44	26.20
Mg	0.93	0.66	4.31
Al	3.71	6.08	4.54
Si	4.83	4.94	1.38
P		1.36	0.21
Ca	29.82	30.82	9.43
Mn	3.20	1.56	7.13
Fe	27.06	22.68	44.91
Total	100	100	100



Fig. 13. A SEM image of the BOF6 sample. The points of the EDS analysis are indicated.

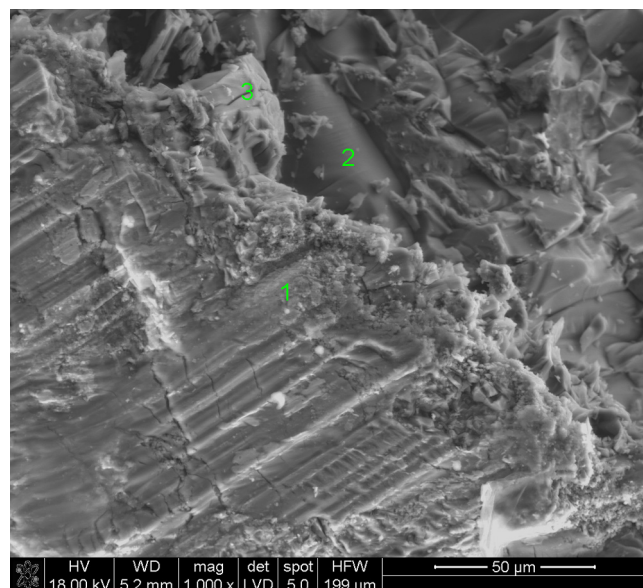


Fig. 14. A SEM image of the BOF2 sample. The points of the EDS analysis are indicated.

Table 8

The results of the EDS analysis of the BOF2 sample from points shown in Fig. 14.

	Point 1 (wt. %)	Point 2 (wt. %)	Point 3 (wt. %)
O	11.11	40.12	39.62
Mg	2.88	0.54	0.54
Al	8.62	18.33	18.99
Si	1.89	11.30	10.88
K	0.40	0.32	0.31
Ca	4.54	24.03	25.71
Ti		0.39	0.18
Mn	5.93	0.63	0.34
Fe	64.14	4.34	3.42
Total	100	100	100

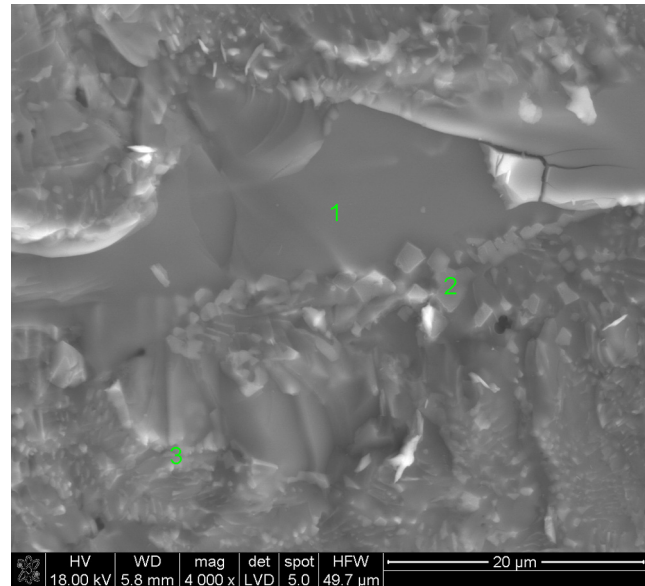


Fig. 15. A SEM image of the BOF5 sample. The points of the EDS analysis are indicated.

Table 9

The results of the EDS analysis of the BOF5 sample from points shown in Fig. 15.

	Point 1 (wt. %)	Point 2 (wt. %)	Point 3 (wt. %)
C	6.22	5.44	6.42
O	26.28	27.18	21.95
Mg		2.30	1.09
Al	18.54	13.53	16.91
Si	10.15	4.72	8.12
K	0.33	0.37	0.20
Ca	30.97	9.93	27.73
Ti		1.17	0.93
Mn		4.30	2.52
Fe	7.51	31.06	14.14
Total	100	100	100

$$\alpha(L^2 \cdot T^{-1}) = \frac{\lambda}{c_p \cdot \rho}$$

where λ is the thermal conductivity, c_p is the specific heat and ρ is the density of the material affected by solar radiation. This parameter, i. e. the thermal diffusivity, can be used as an instrument in the design of an industrial solar process. The design could be based on the displacement of the material below the solar heat source since the thermal diffusivity is related to the speed, v , and the thickness, t , which is affected by the radiation that causes the melting:

$$\alpha = v \cdot t$$

This phenomenon is also related to the presence of a crust of the reacted material of approximately 20 mm in height, while below this layer the material remains unreacted. The presence of this zone of the unreacted material is linked to the capacity of the heat to reach the lower zones of the charge through diffusion mechanisms. It is assumed that once the thermal equilibrium is reached and the reactions have taken place, the remaining time the slag is kept at high temperature and the rest of the heat is re-emitted through the radiation heat transfer mechanism.

4. Conclusions

Concentrated solar energy has a great potential in high temperature applications because of the fast heating rate that could significantly reduce treatment times. Moreover, another advantage of solar energy is that high temperatures are reached without paying for the combustibles as it is the case in the currently used industrial furnaces. On the other hand, BOF slag is a by-product/waste generated in the ironmaking and steelmaking process. The main applications of slags are in road construction and in the manufacture of cement. However, the problem of the BOF slag is that it contains significant quantities of free lime and free magnesia, which makes slag unstable in the presence of water. Stabilizing slag is the first step to the use of BOF slag in the construction industry. Another downside of BOF slag is the presence of significant quantities of iron (14–30 wt%), which is a problem in the production of cement. On its behalf, this iron content becomes BOF slag in an important iron source available in the steel factories. Finally, the third problem is the presence of phosphorus and sulphur, which limits the usability of BOF slag as a recycled material in the iron ore sintering process despite its lime, magnesia, and iron content.

In this project, we treated BOF slag with concentrated solar energy. We observed that the initial free lime and free magnesia combined with the other phases present in the slag to give a product that mainly contained silicates, aluminates, and ferrites. This final product contained neither free lime nor free magnesia, and thus it was not hydrated in the presence of water. The sulphur and most of the phosphorus left the sample during the experiments because in the SEM-EDS analyses neither of these elements was detected (although small amounts of phosphorus were identified in some of the samples). However, the mechanisms capable of eliminating both these elements completely from slag should be further studied, considering that they cannot be released into the atmosphere. Sulphur-and-phosphorus-free BOF slag could be reused in the iron ore sintering process, but it does not seem economically reasonable to develop a process aimed exclusively at the elimination of sulphur and phosphorus. In the case of the iron, it is possible to distinguish two situations: the first, the samples without silica, where we observed that the initial iron (found as FeO and Fe₂O₃) was transformed into maghemite/magnetite; and the second, the samples with 6% wt. silica, where we observed that the initial iron was transformed into fayalite. Therefore, it can be concluded that the additions of silica might limit the recovery of iron from slag. In the other case, maghemite/magnetite are magnetic, so they could be collected using magnetic methods to obtain an iron concentrate. Iron-free slag seems to offer a significant potential as a material to be used in the manufacture of cement and road building.

To conclude, we can say that our main aim was to eliminate the free lime and the free magnesia from the BOF slag. This objective was clearly satisfied (both with and without silica) as neither free lime nor free magnesia were found in the final product. The second objective was the transformation of the iron contained in the slag into a magnetic phase. Magnetite/maghemite were detected as the iron phases in the final product when we did not add silica. However, fayalite was also identified as an iron phase in addition to lower quantities of magnetite/maghemite when we added 6% wt. silica. The objective was satisfied in

the samples where we did not add silica and the magnetic iron oxide could be collected using magnetic methods.

Acknowledgements

This research was supported by the Spanish Ministry of Education, Culture, and Sports via an FPU (Formación del Profesorado Universitario) grant to Daniel Fernández González (FPU014/02436).

The financial support provided by the Access to Research Infrastructures activity in the 7th Framework Program of the EU (SFERA 2 Grant Agreement n. 312643) is gratefully acknowledged and the use of the facilities and its researchers/technology experts. Project SOLMETBY (P1701250238), *Investigation and evaluation of solar energy as energy source in the treatment of metallurgical by-products*.

References

- Annuziata Branca, T., Pistocchi, C., Colla, V., Ragaglini, G., Amato, A., Tozzini, C., Mundersbach, D., Morillon, A., Rex, M., Romaniello, L., 2014. Investigation of (BOF) converter slag use for agriculture in Europe. *Metall. Res. Tech.* 111, 155–167.
- Ballester, A., Verdeja, L. F., Sancho, J. P., 2000. Metalurgia Extractiva. Volume I. Fundamentos, first ed. Síntesis, Madrid.
- Dippenaar, R., 2005. Industrial uses of slag (the use and re-use of iron and steelmaking slags). *Ironmak Steelmak* 32, 35–46.
- Fernández, D., Ordiales, M., Sancho, J., Verdeja, L. F., 2015. Posibilidades de la lógica difusa en operaciones y procesos de la metalurgia primaria. In: Spain Minergy Congress 2015, Gijón/Xixón, Asturias, Spain, 15–19 June 2015.
- Fernández-González, D., Martín-Duarte, R., Ruiz-Bustinza, I., Mochón, J., González-Gasca, C., Verdeja, L.F., 2016. Optimization of sinter plant operating conditions using advanced multivariate statistics: Intelligent data processing. *JOM-J. Min. Met. Mat.* S. 68, 2089–2095.
- Fernández-González, D., Ruiz-Bustinza, I., Mochón, J., González-Gasca, C., Verdeja, L.F., 2017a. Iron ore sintering: raw materials and granulation. *Min. Proc. Ext. Met. Rev.* 38, 36–46.
- Fernández-González, D., Ruiz-Bustinza, I., Mochón, J., González-Gasca, C., Verdeja, L.F., 2017b. Iron ore sintering: process. *Min. Proc. Ext. Met. Rev.* 38, 215–227.
- Fernández-González, D., Ruiz-Bustinza, I., Mochón, J., González-Gasca, C., Verdeja, L.F., 2017c. Iron ore sintering: quality indices. *Min. Proc. Ext. Met. Rev.* 38, 254–264.
- Fernández-González, D., Ruiz-Bustinza, I., Mochón, J., González-Gasca, C., Verdeja, L.F., 2017d. Iron ore sintering: environment, automatic and control techniques. *Min. Proc. Ext. Met. Rev.* 38, 238–249.
- Fernández-González, D., Ruiz-Bustinza, I., González-Gasca, C., Piñuela-Noval, J., Mochón-Castaños, J., Sancho-Gorostiaga, J., Verdeja, L.F., 2018a. Concentrated solar energy applications in materials science and metallurgy. *Sol. Energy* 180, 520–540.
- Fernández-González, D., Prazuch, J., Ruiz-Bustinza, I., González-Gasca, C., Piñuela-Noval, J., Verdeja, L.F., 2018b. Solar synthesis of calcium aluminates. *Sol. Energy* 171, 658–666.
- Fernández-González, D., Prazuch, J., Ruiz-Bustinza, I., González-Gasca, C., Piñuela-Noval, J., Verdeja, L.F., 2018c. Iron metallurgy via concentrated solar energy. *Metals-Basel* 8, 873.
- Ferreira, E.B., Zanotto, E.D., Scudeller, L.A.M., 2002. Glass and glass-ceramic from basic oxygen furnace (BOF) slag. *Glass Sci. Tech.* 75, 75–86.
- Gautier, M., Poirier, J., Bodénan, F., Franceschini, G., Véron, E., 2013. Basic oxygen furnace (BOF) slag cooling: laboratory characteristics and prediction calculations. *Int. J. Min. Process.* 123, 94–101.
- Guo, H., Yin, S., Yu, Q., Yang, X., Huang, H., Yang, Y., Gao, F., 2018. Iron recovery and active residue production from basic oxygen furnace (BOF) slag for supplementary cementitious materials. *Resour. Conser. Recy.* 129, 209–218.
- Kambole, C., Paige-Green, P., Kupolati, W.K., Ndambuki, J.M.N., Adeboje, A.O., 2017. Basic oxygen furnace slag for road pavements: a review of material characteristics and performance for effective utilization in southern Africa. *Constr. Build. Mater.* 148, 618–631.
- Lan, Y., Liu, Q., Meng, F., Niu, D., Zhao, H., 2017. Optimization of magnetic separation process for iron recovery from steel slag. *J. Iron Steel Res. Int.* 24, 165–170.
- Levin, E.M., Robbins, C.R., McMurdie, H.F., 1964. Phase Diagrams for Ceramists. The American Ceramic Society, Columbus, Ohio.
- Menad, N., Kanari, N., Save, M., 2014. Recovery of high grade iron compounds from LD slag by enhanced magnetic separation techniques. *Int. J. Min. Process.* 126, 1–9.
- Mochón, J., Ruiz-Bustinza, I., Vázquez, A., Fernández, D., Ayala, J.M., Barbés, M.F., Verdeja, L.F., 2014. Transformations in the iron-manganese-oxygen-carbon system resulted from treatment of solar energy with high concentration. *Steel Res. Int.* 85, 1469–1476.
- Rabinovich, E.M., 1982. Glass-ceramics from Israeli slag and coal ash. In: Simmons, J.H., Uhlmann, D.R., Beall, G.H. (Eds.), Nucleation and Crystallization in Glasses. American Ceramic Society, Columbus, pp. 334–340.
- Ruiz-Bustinza, I., Cañadas, I., Rodríguez, J., Mochón, J., Verdeja, L.F., García-Carcedo, F., Vázquez, A., 2013. Magnetite production from steel wastes with concentrated solar energy. *Steel Res. Int.* 84, 207–217.
- Sancho, J.P., Verdeja, L.F., Ballester, A., 2000. Metalurgia Extractiva. Volumen II. Procesos de Obtención, first ed. Síntesis.
- Shen, H., Forssberg, E., 2003. An overview of recovery of metals from slags. *Waste Manage.* 23, 933–949.
- Sibieude, F., Ducarroit, M., Tofighi, A., Ambriz, J., 1982. High temperature experiments with a solar furnace: the decomposition of Fe_3O_4 , Mn_3O_4 , CdO . *Int. J. Hydrogen Energy* 7, 79–88.
- Srinivasa Reddy, A., Pradhan, R.K., Chandra, S., 2006. Utilization of Basic Oxygen Furnace (BOF) slag in the production of a hydraulic cement binder. *Int. J. Miner. Process.* 79, 98–105.
- Steinfeld, A., Fletcher, E.A., 1991. Theoretical and experimental investigation of the carbothermic reduction of Fe_2O_3 using solar energy. *Energy* 16, 1011–1019.
- Steinfeld, A., Kuhn, P., Karni, J., 1993. High-temperature solar thermochemistry: Production of iron and synthesis gas by Fe_3O_4 -reduction with methane. *Energy* 18, 239–249.
- TAPP. Version 2.2. ES Microware Inc., Wade Court, Hamilton, OH.
- Zhu, D., Chun, T., Pan, J., Zhang, J., 2013. Influence of basicity of MgO content on metallurgical performances of Brazilian specularite pellets. *Int. J. Miner. Process.* 125, 51–60.